J. Fluid Mech. (1967), *vol.* 27, *part* 2, *pp.* 273–289
Printed in Great Britain

Experiments on the low-speed flow past cones

By J. R. CALVERT
Engineering Department, University of Cambridge

(Received 7 January 1966)

The wake behind a cone in incompressible flow has the form of a closed bubble. Measurements of velocity, turbulence and static pressure for various cone angles show that the wakes are all essentially similar. A wake Strouhal number may be defined, which is the same for all the models. A disk may be treated as a cone of 180° vertex angle.

1. Introduction

There is little published work on incompressible flow past axially symmetric blunt-based bodies. Some experiments were carried out around 1930 (see, for example, Stanton & Marshall 1932), and more recently results have been published by Fail, Lawford & Eyre (1959) and by Carmody (1964) among others. Most of the early work was restricted to flow visualization at low Reynolds numbers. Few results are available for model shapes other than disks and spheres, or for Reynolds numbers above about 1000.

It has been known for some time that there are periodic phenomena associated with such flows, but that these are not nearly so predominant as in two-dimensional configurations. These are presumably related to some kind of regular vortex shedding, but the actual wake pattern is unknown above a Reynolds number of a few hundred.

The experiments reported here provide some information on the wakes behind axisymmetric blunt-based bodies, but knowledge of the flow pattern is still very far from complete.

2. Apparatus

The experiments were carried out in an open return wind tunnel with a working section 20×28 in. The models were supported from downstream on a sting of diameter $\frac{1}{8}$ in. This was held in the centre of the working section by six piano wires of diameter 0·015 in. So that measurements could be made on the centre line, the model was mounted with the sting $\frac{1}{2}$ in. off the centre line for some tests. Comparative measurements showed that this made no appreciable difference to quantities measured off the centre line.

The series of models was as follows:

1. Cones of vertex angle 20°, 40°, 60° and 90°. (These were made of wood, with a base diameter of 2 in.)

2. A brass disk of diameter 2 in. and thickness $\frac{1}{16}$ in. The downstream edge was bevelled at 45°.

Some tests were also made on a cylindrical model of diameter 3 in. and length 9 in., with an ellipsoidal nose 4 in. long fitted with a transition ring. This model was also held in the working section by an arrangement of wires.

Velocities were measured with a DISA constant temperature hot-wire anemometer. The probe wire was normal to the free-stream direction and along a radius of the wake.

Frequencies were measured by passing the output from the anemometer through a frequency analyser. This was coupled to an X–Y plotter in such a way that a frequency spectrum could be obtained.

Static pressures were measured with a static tube aligned in the free-stream direction. The base pressures of the cones were measured by putting a Pitot tube into a small hole in the base, that of the disk by putting a Pitot tube close to the base. The cylindrical model was provided with a pressure tapping hole in the centre of the base.

3. Experiments

For each model, measurements were made of the base pressure and the variation of static pressure along the centre line of the wake. Traverses with the hot wire were made along the wake centre lines and across diameters of the wakes at various longitudinal positions, including those of the minima of the static pressure traverses. Frequency spectra of the hot-wire output were taken at various positions in the wakes. The Reynolds number of most of the observations was around 5×10^4, based on maximum diameter.

Some visual observations of the flow past a disk were made in a smoke tunnel at a Reynolds number of about 1000. The flow past the 60° cone was examined at the higher Reynolds number of 5×10^4, using a wool tuft.

4. Interpretation of results

4.1. *Calibration assumed for hot wire*

The output of the anemometer is in the form of a voltage V which is proportional to the mean voltage across the wire, and a voltage v which is proportional to the root mean square of the fluctuating component of the voltage across the wire.

The basic calibration used was the King's law equation for constant wire resistance $V^2 = \alpha + \beta U^{\frac{1}{2}}$, where V and U are the voltage and velocity in steady flow and α and β are constants. This can be expressed in the form

$$\frac{U}{U_\infty} = \left(\frac{V^2 - V_0^2}{V_\infty^2 - V_0^2}\right)^2, \tag{1}$$

where V_∞ and U_∞ are the free-stream values of V and U, and V_0 is the value of V for no flow. Calibration of a probe in the empty wind tunnel showed no significant deviation from this law between the maximum speed used in the present experiments and the lowest speed which could be accurately measured. The intercept at $U = 0$ corresponded closely with the measured value of V_0.

It was assumed that in unsteady flow (1) would be valid both for instantaneous and for mean quantities. The latter assumption is not strictly true, but the

maximum error in U/U_∞ in a typical traverse is likely to be small compared to that involved in later assumptions.

We may define two functions of the anemometer output: θ and ϕ, such that

$$\theta = 4vV\frac{V^2 - V_0^2}{(V_\infty^2 - V_0^2)^2} \times 100 \tag{2}$$

and

$$\phi = \frac{4vV}{(V^2 - V_0^2)} \times 100. \tag{3}$$

With the assumptions that $(\overline{u^2})^{\frac{1}{2}} \ll U$ and $v \ll V$ (where u is the perturbation velocity) it follows from King's law that

$$\theta = \frac{(\overline{u^2})^{\frac{1}{2}}}{U_\infty} \times 100 \quad \text{and} \quad \phi = \frac{(\overline{u^2})^{\frac{1}{2}}}{U} \times 100.$$

It was assumed that these relations would hold even when $(\overline{u^2})^{\frac{1}{2}}/U_\infty$ and $(\overline{u^2})^{\frac{1}{2}}/U$ were not small, and that θ and ϕ would thus always be representative of the unsteady component of the flow.

In all the above equations, u and U refer strictly to the component of velocity normal to the wire. If the components of velocity in the free-stream direction are denoted by u_1 and U_1, work by Hoole & Calvert (1966) has shown that a smoothed curve through the experimental points of U/U_∞ is a good approximation to U_1/U_∞. The quantity ϕ also is a good estimate of $(\overline{u_1^2})^{\frac{1}{2}}/U_1$. The quantity θ is found to lie between $(\overline{u_1^2})^{\frac{1}{2}}/U_\infty$ and q/U_∞, where q is the total perturbation speed. Since the evaluation of the individual components of the velocity involves considerably more experimental and computational work, all results are expressed in terms of U/U_∞, θ and ϕ as defined above in (1), (2) and (3). θ may thus be taken as a measure of the level of velocity fluctuations for the purpose of comparison between models, but too much meaning should not be attached to its numerical value. The smoothed curves of U/U_∞ and ϕ are probably more meaningful, although the experimental points may be expected to deviate from the curves in regions of high turbulence and low mean velocity.

V_0 and V_∞ were measured after each traverse. It was assumed that they did not vary (due to dust collection or other causes) during any traverse. This assumption was supported by the fact that V_0 was found to change little from day to day.

4.2. *Other assumptions made*

Effects of unsteadiness of flow on the reading of the static tube were ignored. It was assumed that the mean flow pattern was axisymmetric and that there was no mean circumferential flow. The assumption of axial symmetry is supported by the tuft and smoke observations, and also by the fact that all the diametrical traverses were symmetrical about the centre line, irrespective of their axial position, the model or the occasion on which they were measured. If the wakes were not axially symmetric it would be expected that some at least of these traverses would be unsymmetrical. This was observed when the models were deliberately yawed (see §9).

5. Co-ordinate system

The origin is at the centre of the model base. (For the disk, it is at the centre of the upstream face.) The x-axis is in the axial direction, positive downstream. The y-axis is radial.

6. Blockage and interference effects

For various reasons, it was impossible to keep the traverse gear and support systems the same for all measurements on all models, so the effect of modifying them for any one model was investigated. It was found that Strouhal number and base pressure varied somewhat, while wake width and the general shape of the velocity and pressure traverses did not change significantly. The wake Strouhal number (see § 10) was not affected.

This kind of effect is similar to that which would be expected from a small amount of wind-tunnel blockage. Presumably, normal blockage effects are also present and will vary from one model to another. These were noticed when some of the tests were repeated on a 60° cone with 3 in. base diameter. It is assumed that all blockage and interference effects may be considered together as equivalent to a single blockage.

Most blockage theories make the assumption that the principal effect is an increase in free-stream velocity, and consequent fall in static pressure. A similar result could be produced by a suitable change in body geometry, so that blockage and interference effects may be considered as modifications of the shape of the model. Actual model geometry plays no part in any conclusions presented here, so that the effects are irrelevant. It is assumed, however, that the magnitude of the effects is fairly small, and that there is no significant departure from axisymmetry.

In the following, all directly measured quantities are presented uncorrected for blockage. All the results for any one model were measured under similar conditions, but conditions varied somewhat between one model and another. Numerical values given are as measured; these may vary considerably with changes in blockage and interference. For these reasons, direct comparison between models is hazardous. However, it has been found (by modifying the traverse gear arrangement for a given model) that some of the reduced results are apparently independent of blockage effects. These are indicated where they appear in the text.

7. Mean flow pattern

From the results of Fail *et al.* (1959) and Carmody (1964) and by analogy with two-dimensional base flows, it seems clear that the main feature of flows of this type is a recirculating bubble flow. This conclusion is reinforced by the smoke and tuft observations, and such a flow is sketched in figure 1. The hot-wire anemometer gives no indication of the sign of the velocity, and the sign at each experimental point must be decided by inspection. On the assumption of the above

flow model, there is a stagnation point downstream of the base with reversed flow between it and the base.

In conditions where there are very strong periodic motions, these dominate the wake. It is then unlikely that the mean flow pattern is very meaningful. In the present cases, the periodic motions are weak (see § 10) and the mean flow pattern may be significant.

A measure of the relative importance of the mean and periodic parts of the flow will be given by the scale of the unsteadiness in the region of the stagnation

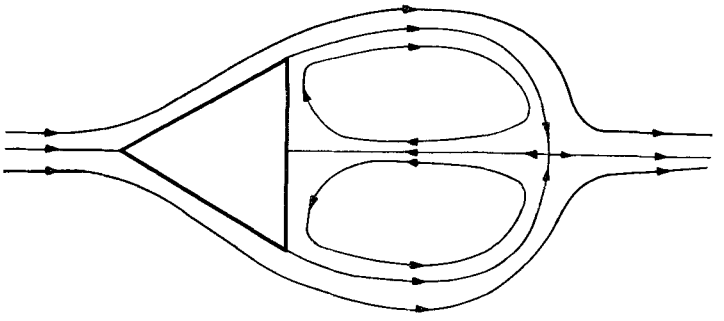

FIGURE 1. Sketch of probable mean flow pattern.

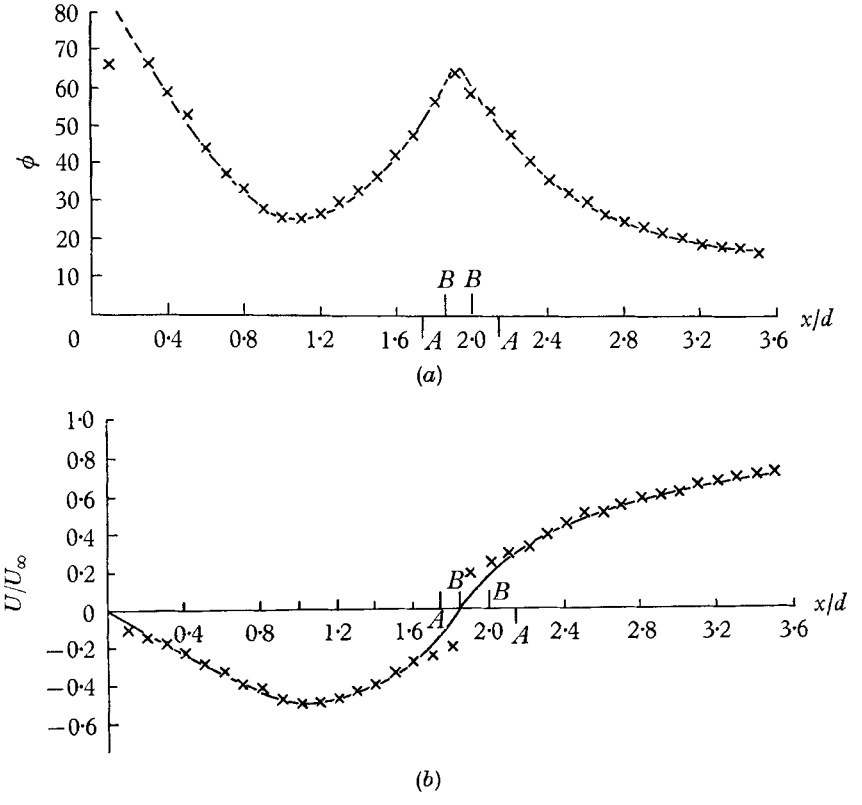

FIGURE 2. (*a*) Longitudinal variation of velocity fluctuations in terms of local mean velocity behind 60° cone. (*b*) Longitudinal variation of mean velocity behind 60° cone.

point. A suitable variable is the quantity ϕ, which is assumed (see §4, 1) to be everywhere proportional to the ratio of local r.m.s. velocity fluctuations to local mean velocity ($\phi = (\overline{u^2})^{\frac{1}{2}}/U \times 100$). Figures 2 (*a*) and (*b*) show the distribution of ϕ and mean velocity respectively along the axis of the wake of the 60° cone. It

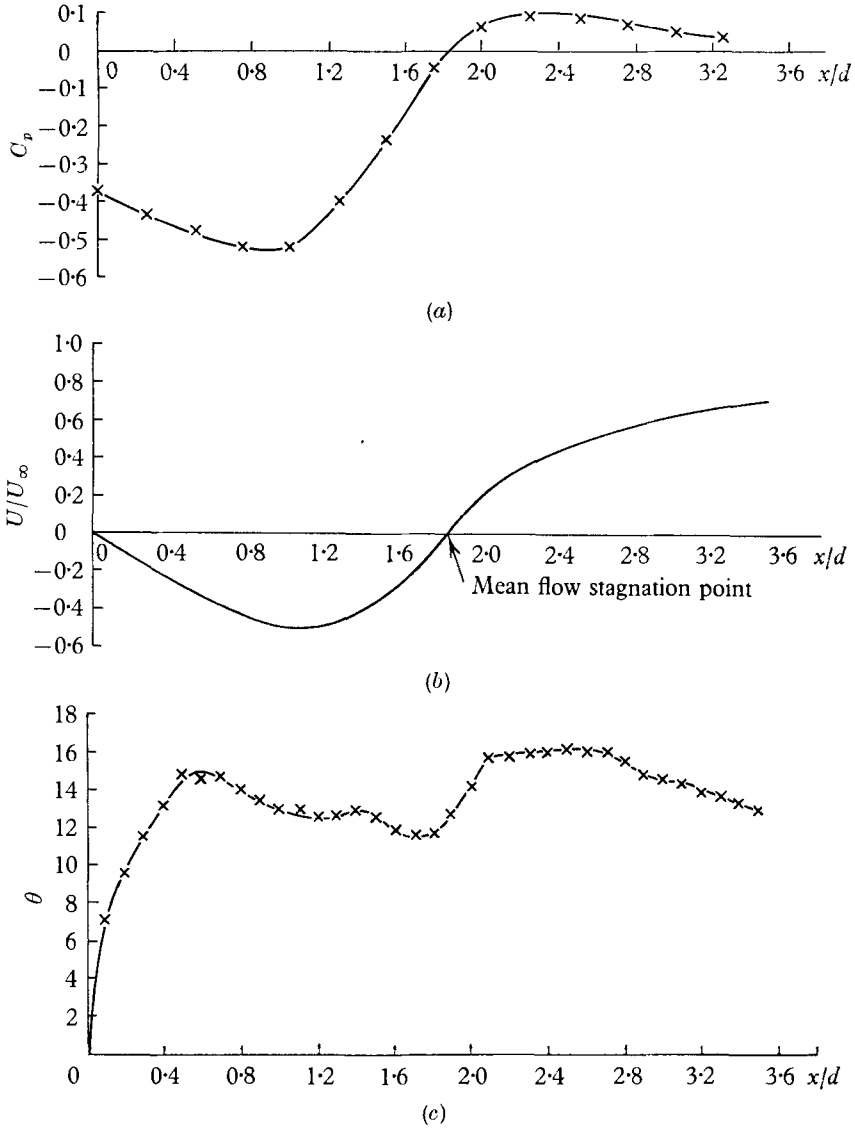

FIGURE 3. (*a*) Longitudinal variation of static pressure behind 60° cone. (*b*) Longitudinal variation of mean velocity behind 60° cone. (*c*) Longitudinal variation of velocity fluctuations in terms of free-stream velocity behind 60° cone.

will be seen that the value of ϕ at the centre of the bubble is about 25. Therefore a reasonable criterion for the size of the area around the stagnation point in which the flow is more unsteady than elsewhere would be the region in which ϕ is greater than 50. The axial length of this region (AA in figure 2) is about $0{\cdot}40d$,

where d is the base diameter. This is equivalent to about $0{\cdot}22X$, where X is the bubble length. For ϕ greater than 60 it is $0{\cdot}08X$ (*BB* in figure 2). The critical levels chosen are rather arbitrary, but the values are small enough to indicate that the mean flow pattern probably has some significance.

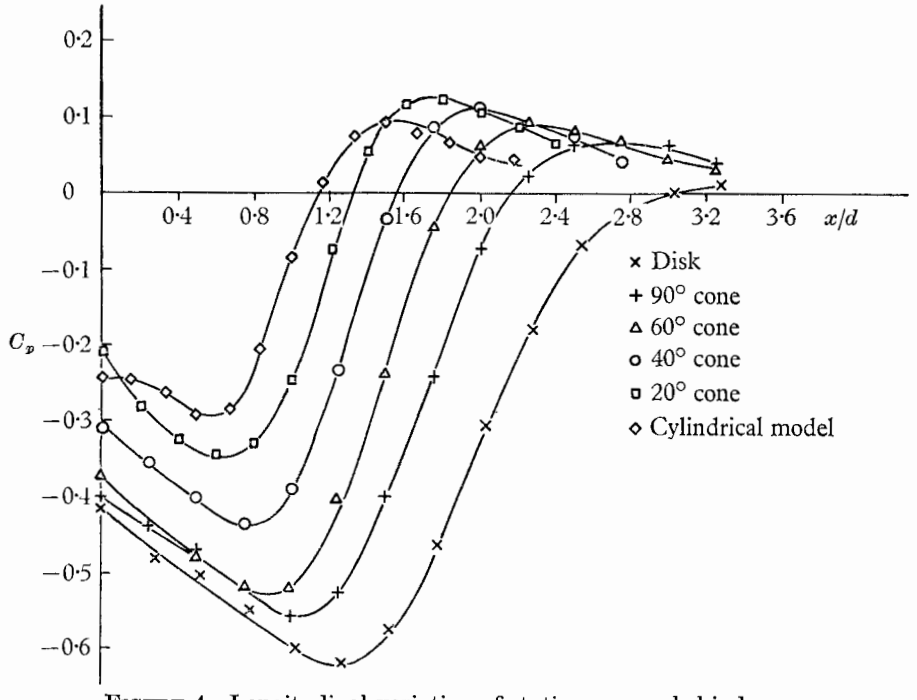

FIGURE 4. Longitudinal variation of static pressure behind cones.

8. Streamwise traverses

Results for the 60° cone, which are typical, are shown in figure 3. The static pressure (figure 3*a*) reaches a minimum value a little way downstream of the base, and rises to a maximum (above free-stream static pressure) downstream of the mean flow stagnation point. It presumably reaches free-stream static pressure far downstream.

The static pressure coefficient is zero at the stagnation point. This is nearly true for all the models, the maximum distance between the point at which $C_p = 0$ and the stagnation point being $0{\cdot}3d$ ($0{\cdot}12X$) for the disk. For the 90° cone it is $0{\cdot}1d$ ($0{\cdot}05X$). For all the other models it is zero within the limits of experimental error. This result is rather surprising, and the reason for it is not obvious. It may be purely fortuitous, but this seems unlikely.

In general, the base, minimum and maximum pressures rise as the cone angle falls. The cylindrical model has lower maximum and base pressures than might be expected; this is probably due to the very much thicker boundary layer. The base pressure coefficients C_{pB} ranged from $-0{\cdot}21$ to $-0{\cdot}41$ through the range of models. The static pressure distributions for all the models are shown in figure 4 and the base pressures are shown in table 1.

The mean velocity curve (figure 3*b*) is drawn on the assumption of reversed flow in the bubble, as described in §7, above. The points near the stagnation point do not lie on the smoothed curve, for the reasons given in §4.1.

The maximum reversed velocity coincides approximately with the static pressure minimum, and is about $0{\cdot}5U_\infty$. It is less for the cylindrical model and for one measurement for the 20° cone (see §11.3). The bubble length decreases with cone angle.

Cone angle	$-C_{pB}$	S	d'/d	S^*
0 (cylindrical)	0·244	0·246	0·885	0·195
20	0·210	0·207	1·00	0·188
40	0·310	0·197	1·12	0·193
60	0·375	0·171	1·29	0·188
90	0·400	0·163	1·42	0·196
180 (disk)	0·413	0·135	1·65	0·187

TABLE 1. Variation of base pressure, Strouhal number and wake width with cone angle

The axial distributions of θ (figure 3*c*) show two maxima, one near the static pressure minimum and one near the maximum. The small variations in magnitude which can be seen between the two maxima appear to some extent on most of the curves. In general the height of the first peak was about $\theta = 15$, that of the second $\theta = 16$. The intermediate minimum was about $\theta = 11{\cdot}5$. The cylindrical model and one traverse for the 20° cone showed rather lower values (see §11.3). However, the exact shape and level of these curves is to a large extent governed by the anemometer response.

9. Diametrical traverses

The diametrical mean and fluctuating velocity distributions fall into two groups: those upstream of the stagnation point and those downstream of it.

A typical example of the first type is shown in figure 5. The mean velocity shows, by the same arguments as in §7, a large reversed velocity in the centre. On each side there is a rapid rise to a value above free-stream velocity at the edge of the wake. Points in the region of $U/U_\infty = 0$ are not on the curve, for reasons given in §4.1. The hot wire is primarily sensitive to the velocity normal to itself, and it is likely that the smoothed curve shown is a good estimate of the velocity component in the free-stream direction.

The value of θ is low outside the wake and rises to a sharp peak, presumably in the free shear layer. It has minima near the points $U/U_\infty = 0$ and on the centre line. The two main peaks are in the region where U/U_∞ is changing most rapidly. Here again, the anemometer response will have a significant effect on the details of the results.

As it was difficult to align the models very accurately in the free-stream direction, the effect of small amounts of yaw (of the order of 1° or 2°) was investigated.

It was found that although the symmetry of the distributions was affected, and there was some lateral displacement, the transverse length scale was not altered.

Downstream of the stagnation point the profiles are somewhat different (figure 6). The mean velocity no longer rises above the free-stream value and of

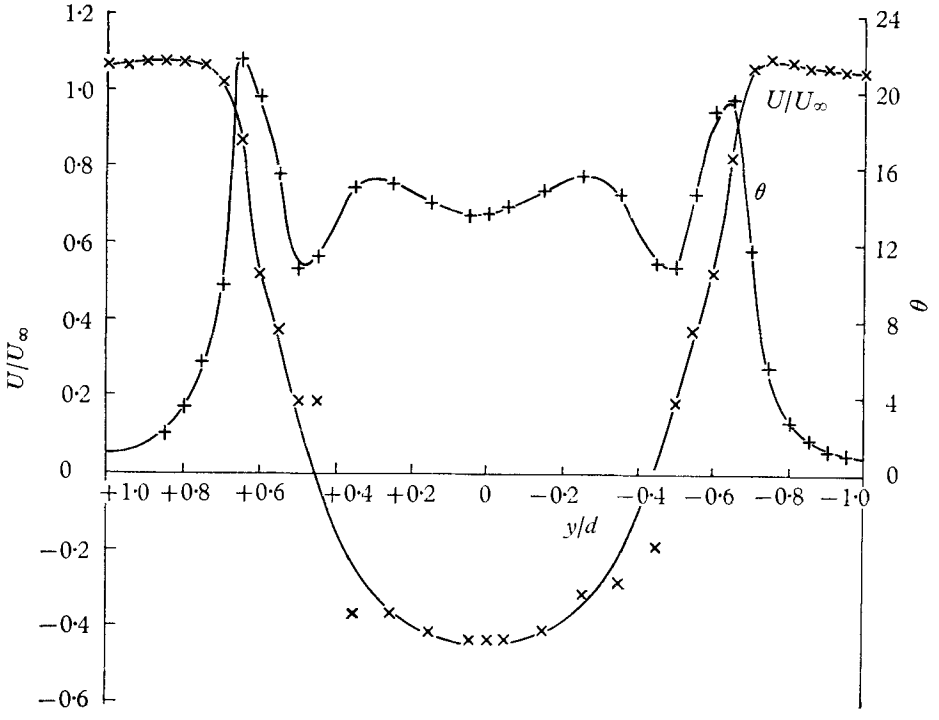

FIGURE 5. Variation of mean velocity and velocity fluctuations across wake of 60° cone. $x/d = 0{\cdot}88$.

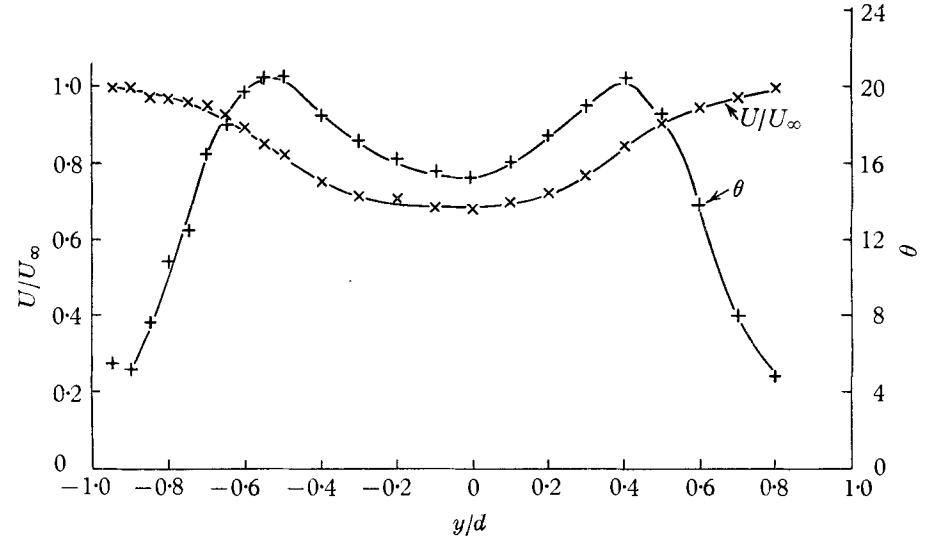

FIGURE 6. Variation of mean velocity and velocity fluctuations across wake of 60° cone. $x/d = 2{\cdot}5$.

course does not fall below zero. The two main peaks of θ are no longer so prominent, and the two lesser ones have disappeared entirely.

The distance between the main peaks of θ varies with axial distance. It seems to be a maximum near the static pressure minimum (where, according to the smoke observations, the bubble width is a maximum). It falls to a minimum somewhere downstream of the stagnation point and then starts to increase slowly. In the case of the cylindrical model, the minimum width is at about the same streamwise position as the static pressure maximum (and the second peak of θ). For the other models, it moves downstream as the cone angle is increased. The variation is not large. For the 60° cone, the minimum width is about 70 % of the maximum.

10. Periodic phenomena

The output from the anemometer was fed through a frequency analyser to an X–Y plotter, so that a frequency spectrum of the velocity fluctuations was obtained. Any discrete frequency present should show up on this spectrum, although the exact shape of the peak will depend on the characteristics of the analyser.

If a quick traverse across the frequency spectrum is made, the results are rather erratic and unrepeatable. However, if the traverse is made slowly, covering the range of fd/U_∞ (where f is frequency) from about 0·01 to about 10 in 2–3 min, consistent results are obtained. Spectra measured in the wake show a large amount of random 'noise', but in certain areas a definite peak may be seen. The frequency n of this peak varies somewhat between successive determinations; the Strouhal number $S = nd/U_\infty$ may vary by as much as ± 5 % from its mean; but if an average over six or eight measurements is calculated, reasonably consistent and repeatable results are obtained. Such an average is used in the subsequent calculations. The frequency does not vary from place to place in the wake. The Strouhal numbers are shown in table 1. Figure 7 shows a spectrum for the 60° cone.

The peak is only discernible in the wake. It is most prominent in the region of the static pressure maximum, and is undetectable upstream of the static pressure minimum. Nowhere is it sufficiently strong to be identified by inspection of an oscilloscope trace.

The existence of this peak is taken to mean that there is some kind of regular vortex shedding in the wake. The actual pattern of the vortices is not known, and, in view of the highly unsteady nature of the flow, its determination presents many difficulties. The simplest approach would probably be the statistical correlation of two or more signals filtered at the peak frequency. This has not been attempted in the present work.

From these results, it seems that the periodic wake first appears in the region of the static pressure minimum. This conclusion is qualitatively confirmed by smoke observations of the flow past a disk at low Reynolds number. The periodicity presumably arises from instability of the free shear layer in an adverse pressure gradient.

If the periodicity is generated in the region of the static pressure minimum, conditions there should have a large effect on the periodic wake. Fail *et al.* (1959) have shown that, for a disk, the static pressure just outside the wake at this position is about the same as the base pressure. The local velocity will thus be $U_m = U_\infty(1-C_{pB})^{\frac{1}{2}}$, and it seems reasonable to use this velocity to form the Strouhal number. If a wake diameter d' is defined as the distance between the major peaks of a diametrical traverse of θ taken at this axial position, a wake

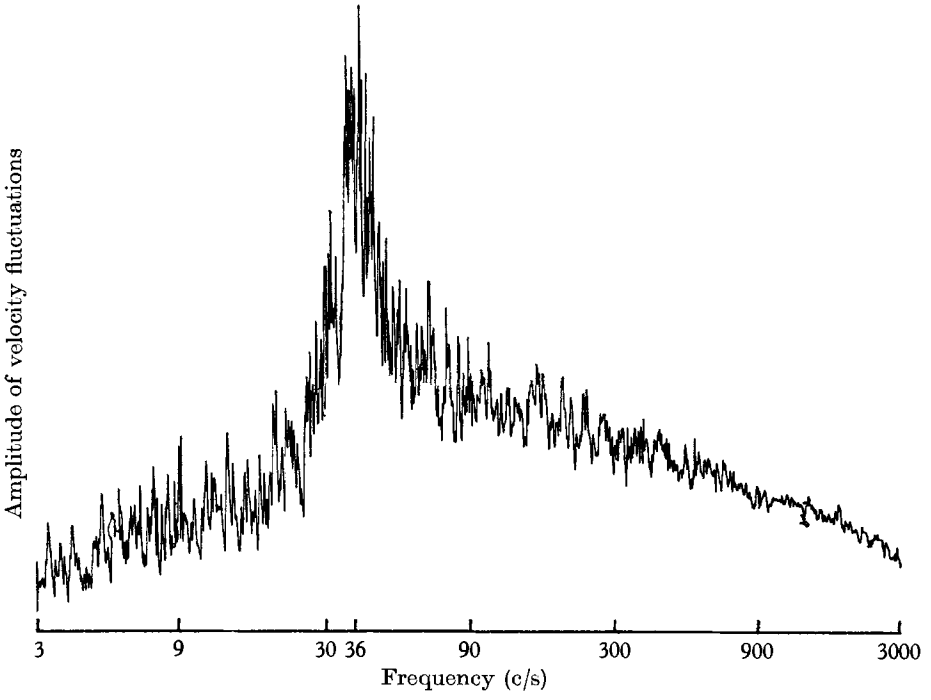

FIGURE 7. Spectrum in wake of 60° cone.

Strouhal number $S^* = nd'/U_m = S(1-C_{pB})^{-\frac{1}{2}}(d'/d)$ may be formed. It was found that this quantity had a constant value of 0·19 (within the limits of experimental scatter) for all the cones, the disk and the cylindrical model. Values of S^* and d'/d are given in table 1. It was also found, by varying the traverse gear and support configurations for several of the models, that this value was independent of blockage. The definition of S^* is the same as that used by Roshko (1955) except that the wake width is differently defined.

It was noticed that the wake width d' was closely equal to the width at which $U/U_\infty = 0{\cdot}6$, for all models.

11. Wake similarity

11.1. *Diametrical traverses*

Carmody (1964) has shown that similarity profiles exist for the mean and fluctuating velocities across diameters of the wake some way downstream of a disk. It has been found that such profiles exist for the wakes of the family of cones. The variables used are as follows: for θ, $\bar{\theta} = \theta/\theta_{\max}$, where $\theta_{\max}$ is the maximum

value of θ on any given traverse, and $y_1 = y/y_t$, where y_t is the value of y at which $\overline{\theta} = 0{\cdot}5$. For U/U_∞ the variables are $\overline{U} = (U - U_c)/(U_\infty - U_c)$ where U_c is the value of U on the centre line for any given traverse, and $y_2 = y/y_m$, where y_m is the value of y at which $\overline{U} = 0{\cdot}5$. These profiles are shown in figures 8 and 9 for $\overline{U}$ and $\overline{\theta}$ respectively. For clarity, only representative experimental points are shown.

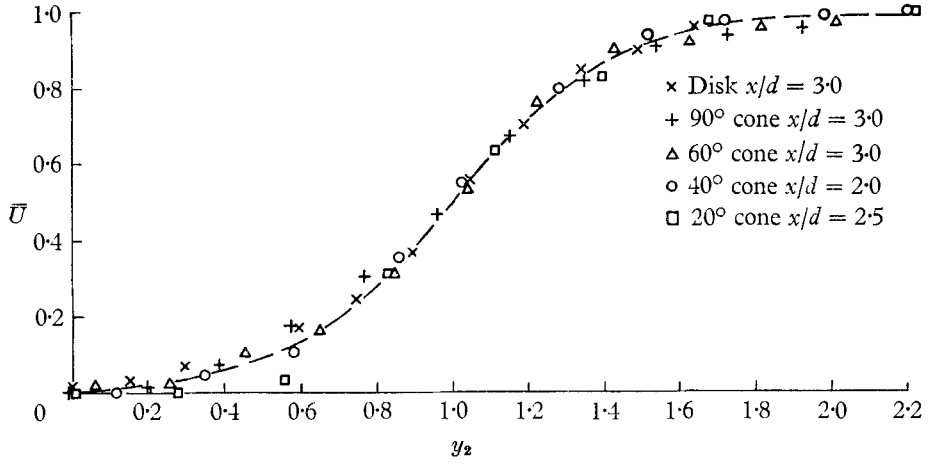

FIGURE 8. Diametrical similarity profile for mean velocity.

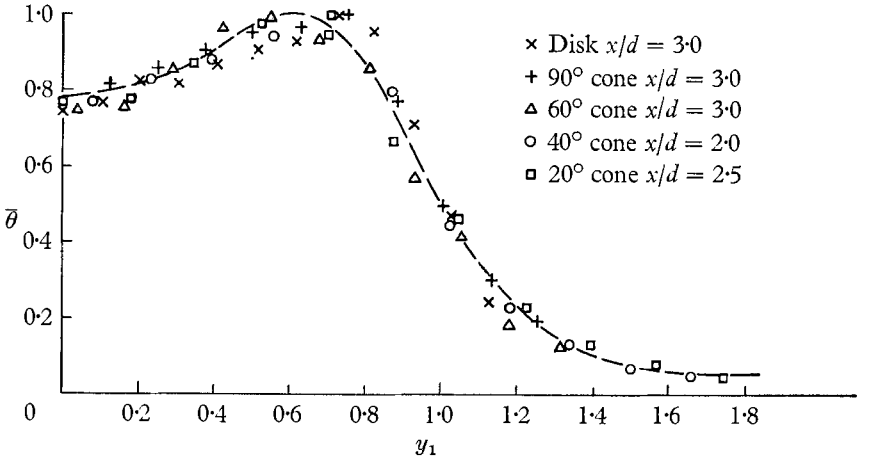

FIGURE 9. Diametrical similarity profile for velocity fluctuations.

It was found experimentally that $y_t \doteqdot 1{\cdot}5y_m$, so that the scale on figure 8 is $1\frac{1}{2}$ times that on figure 9.

The figures show the profiles for traverses across the wakes of all the cones and the disk at various streamwise positions. All the data measured downstream of the stagnation points lie on these curves, as do Carmody's results for a disk. Upstream of the stagnation point the curves of $\overline{U}$ and $\overline{\theta}$ do not collapse on to these curves or on to each other.

Fail *et al.* (1959) give a curve showing the variation of θ across a diameter of the wake of a disk. Although it was downstream of the stagnation point, their

points do not lie on the curve obtained in the present experiments. The reason is probably that their traverse was too close to the stagnation point; the shape of their curve is intermediate between the two characteristic shapes illustrated in figures 5 and 6.

They also give a curve for a traverse of θ across the wake of a two-dimensional flat plate. The results fit on to the present curve except in the outer region of the wake. The agreement is probably fortuitous, but may be significant. The difference in the outer part could be due to the differences in free-stream turbulence.

The curves of $\overline{U}$ and $\overline{\theta}$ reach their free-stream values at about $y_2 = 2{\cdot}0$ and $y_1 = 2{\cdot}0$ respectively and the maximum value of $\overline{\theta}$ occurs at about $y_1 = 0{\cdot}6$.

The restraints put on the curves by the co-ordinate system are that they shall both pass through the point (0·5, 1·0) and touch the lines $\overline{\theta} = 1{\cdot}0$ (at $\theta = \theta_{\max}$) and $\overline{U} = 1{\cdot}0$ (in the free stream) respectively. The $\overline{U}$ curve must pass through the origin, and by symmetry the curves must have zero slope at $y_1 = 0$ and $y_2 = 0$.

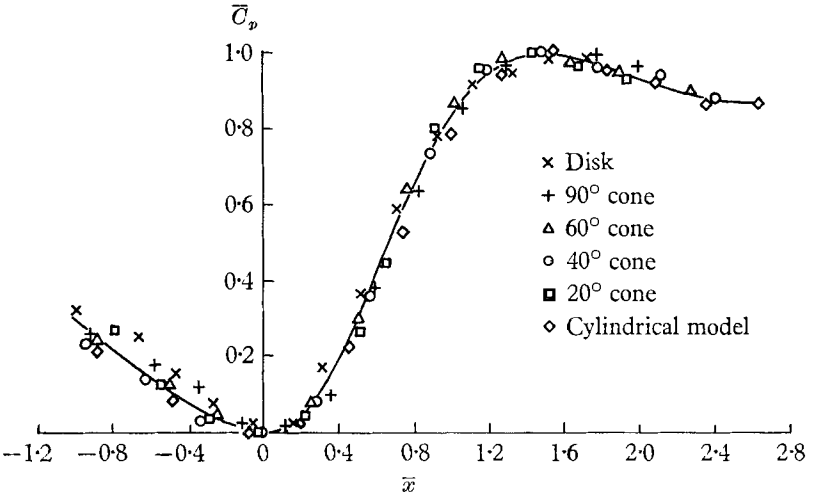

FIGURE 10. Longitudinal similarity profile for static pressure.

11.2. *Longitudinal traverses*

11.2.1. *Static pressure*

Roshko & Lau (1965) have made most of their results for the static pressure distributions downstream of two-dimensional steps collapse on to one curve by the use of the variables $(C_p)_1 = (C_p - C_{pB})/(1 - C_{pB})$ and $x_1 = x/x_r$, where x_r is the reattachment distance. In the present case the corresponding variables are $(C_p)_1$ as above and $x_2 = x/X$, where X is the distance from the base to the stagnation point. This reduction does not, however, lead to a collapse of the data. Roshko & Lau found little difference between their base and minimum pressures, while here the difference is appreciable. If the results are referred instead to the minimum pressure, using $(C_p)_2 = (C_p - C_{p\,\min})/(1 - C_{p\,\min})$ and $\overline{x} = (x - x_m)/(X - x_m)$ ($C_{p\,\min}$ is the minimum pressure and x_m its longitudinal position) the collapse is better. The maxima all come to about the same streamwise position, and the curves are of similar shape, but there are some differences in magnitude. The curves for the cones of smaller angle tend to fall below those of larger angle.

If the curves are scaled up to the same maximum pressure (using $\bar{C}_p = (C_p - C_{p\,\min})/(C_{p\,\max} - C_{p\,\min})$, where $C_{p\,\max}$ is the maximum pressure) there is good collapse for the static pressure results for all the models (figure 10). The maximum pressure is at $\bar{x} = 1{\cdot}5$, the base about at $\bar{x} = -1{\cdot}0$. The base pressure coefficient corresponds approximately to $\bar{C}_p = 0{\cdot}3$. The pressure coefficient at the stagnation point and far downstream corresponds approximately to $\bar{C}_p = 0{\cdot}85$.

11.2.2. *Mean velocity*

From the above it is clear that $\bar{x}$ is a relevant length scale for the early part of the wake. Figure 11 shows the axial traverses of U/U_∞ plotted against $\bar{x}$. Downstream of the stagnation point, agreement is reasonable between all the models. Upstream of it, there are marked differences in the magnitude of the reversed

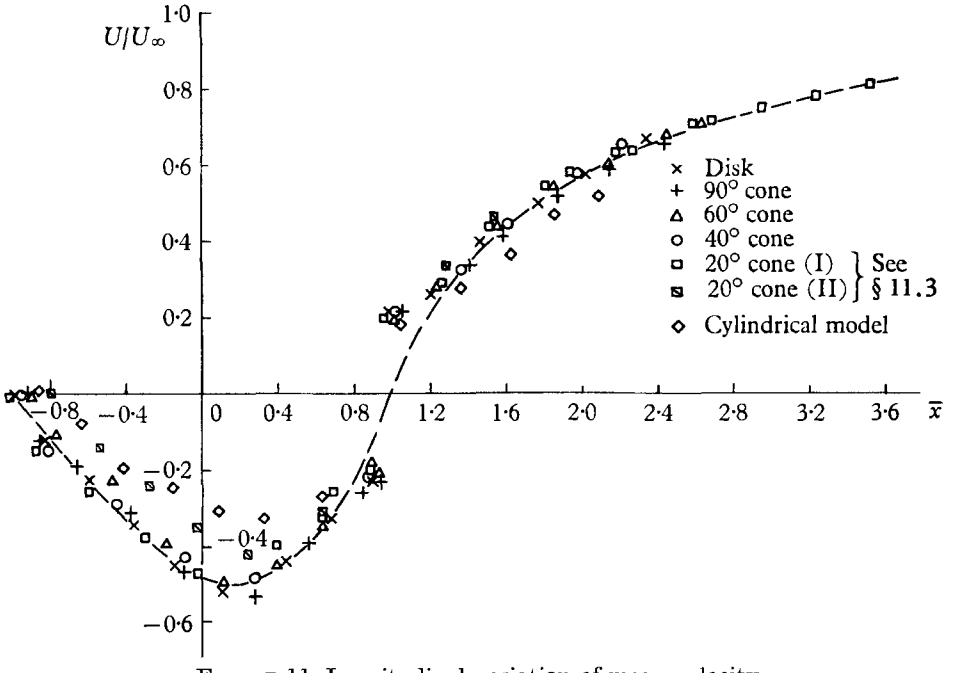

FIGURE 11. Longitudinal variation of mean velocity.

velocity, although the positions of the maximum values agree quite well. The 20° and cylindrical models have lower reversed velocities than the others. If the curves are scaled up to the same maximum value of reversed velocity, agreement in the bubble is better but downstream of the stagnation point there is considerable deviation. It thus appears that the parts of the wake upstream and downstream of the stagnation point require different scales of velocity; the former based on the maximum reversed velocity and the latter on free-stream velocity.

11.2.3. *Velocity fluctuations*

Figure 12 shows the corresponding plots of θ against $\bar{x}$. Here again, there is reasonable agreement between all models except the 20° cone and the cylindrical model, which have lower values. Agreement is not so good downstream of $\bar{x} = 1{\cdot}2$. The curves have, however, much the same shapes, and some observations may

be made. The two peaks occur at about $\bar{x} = -0{\cdot}4$ and $1{\cdot}5$, the latter being coincident with the static pressure maximum. The minimum is at about $\bar{x} = 0{\cdot}9$.

The results of the last two sections are, of course, affected by the blockage considerations discussed in §6. The collapsed diametrical and static pressure curves are not; they depend on the shape of the distributions rather than their magnitude.

Only a few representative experimental points are shown in figures 10, 11 and 12. The restraints placed on the curves by this system of co-ordinates are that the curves of $\bar{C}_p$ must pass through the origin, reaching a minimum there, and touch the line $\bar{C}_p = 1{\cdot}0$ at their maxima. The curves of U/U_∞ must pass through the point $U/U_\infty = 0$, $\bar{x} = 1{\cdot}0$. There are no restraints on the curves of θ.

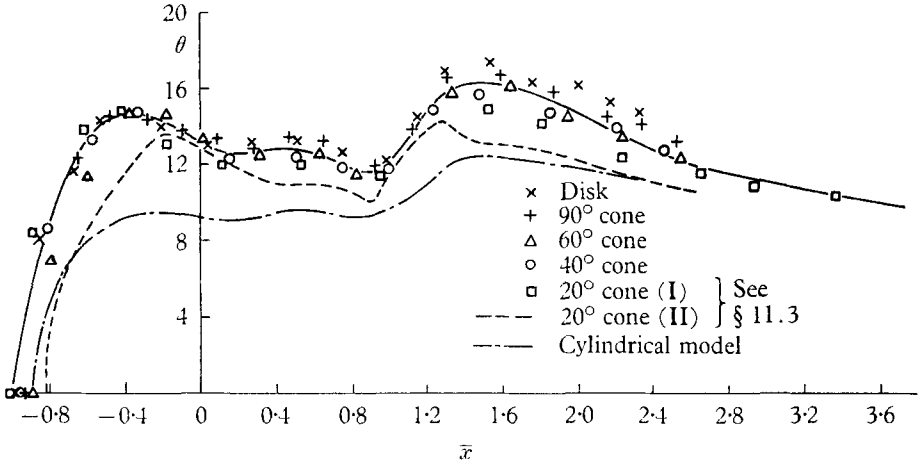

FIGURE 12. Longitudinal variation of velocity fluctuations.

11.3. *Effects of model vibration*

It was found that the static pressures for the 20° cone were considerably lower than for the others in the region between the base and the static pressure minimum. This model was longer and heavier than the others, and when mounted in the same manner could sometimes be seen to vibrate. It was suspected that this vibration was responsible for the discrepancy, and the mounting was made more rigid. The streamwise traverses were repeated, and it was found that the static pressure measurements then agreed well with the collapsed curve. It is these points which are shown in figures 4 and 10. The mean velocity and velocity fluctuations, however, agreed less well than previously. The mean velocity curve was the same shape as before, but reduced in magnitude in the bubble region. The θ curve was also reduced in magnitude, and seemed to be slightly contracted in a streamwise direction in the latter half of the bubble region. Both the original and the new points are shown on figures 11 and 12. The Strouhal number and d'/d were also re-measured. They were found to be slightly changed, but the effect on them and on the wake Strouhal number was within the normal scatter of results.

12. Discussion of results and conclusions

It appears that, for many purposes, the disk and the cylindrical model can be considered as cones of vertex angle 180° and 0° respectively.

The wakes show a definite periodicity which is, however, not nearly so marked as in two-dimensional base flows at the same Reynolds numbers. The frequency can be described by a suitably defined wake Strouhal number S^*, which is found to have a value of 0·19 for all the models tested. The work gives no information on the geometrical form of the periodic wake; only its frequency has been measured.

Despite the periodicity, the mean flow pattern is significant. The configuration is a closed bubble of reversed flow behind the body, with a stagnation point which, although unsteady, remains a fairly constant distance downstream of the base.

The static pressure coefficient is closely equal to zero at the stagnation point for all the models. This is as yet unexplained.

The wake may be divided into two regions: upstream of the stagnation point and downstream of it. In the latter region, the wake is fully developed. The diametrical profiles of mean and fluctuating velocity are similar for all cones and all streamwise positions, and are not markedly different from those for two-dimensional flows. They can be made to collapse on to one another. In the former region, the wake is in the process of formation. The minimum static pressure on the axis is at about the mid-point of the bubble, and coincides approximately with the maximum bubble width. The periodic motion first appears around the static pressure minimum. The shape of the diametrical traverses varies somewhat with streamwise position, and they cannot be collapsed. However, traverses for different models at corresponding positions are of similar shapes.

With a suitable definition of origin and streamwise length scale, the distributions of static pressure, mean velocity and velocity fluctuations in the free-stream direction for the various models can be made to agree in length, although there are discrepancies in magnitude. The static pressures can be collapsed by scaling them to the same maximum and minimum values, and the agreement continues well downstream of the stagnation point. The hot-wire traverses cannot apparently be collapsed so satisfactorily.

It is found that the scales of length used to form the wake Strouhal number (d'/d) and to collapse the streamwise traverses $(X-x_m)/d$ are linearly related. The relation is approximately $d'/d = 0{\cdot}13 + 1{\cdot}2(X-x_m)/d$.

There is no obvious relation between the magnitudes of the various measured quantities and the cone angle. In general pressure coefficients, velocities and Strouhal numbers fall and dimensions increase as cone angle increases. They are all, however, probably influenced to a greater or lesser extent by separation boundary layer thickness (itself a function of cone angle), vibration and blockage.

In brief, the wakes behind these cones are all essentially similar, both in the near and distant regions, and in the frequency of their periodic structures.

REFERENCES

CARMODY, T. 1964 *J. Basic Engng.* Trans. ASME, 86-D-4, 869.

FAIL, R., LAWFORD, J. A. & EYRE, R. C. W. 1959 *Aero. Res. Coun. R & M* no. 3120.

HOOLE, B. J. & CALVERT, J. R. 1966 Cambridge University Engineering Laboratory. Unpublished.

ROSHKO, A. 1955 *J. Aero. Sci.* **22**, 124.

ROSHKO, A. & LAU, J. C. 1965 GALCIT Pasadena publication no. 605. *Proc.* 1965 *Heat Trans. and Fluid Mech. Inst.* Stanford University Press.

STANTON, T. E. & MARSHALL, D. 1932 *Aero. Res. Coun. R & M* no. 1358.